Paper Title

Enhanced Cr(VI) Adsorption on Nitrogen and Sulfur Functionalized Granular Activated Carbon

Authors

Ali Bakhshi-Zadeh[a], Janelle Balzer[a], Negar Fahimi[a], Nael Yasri[a], Linda J. Eastcott[b], Krista Stevenson[b], Edward PL Roberts[a], Anne M. Benneker[a], Sathish Ponnurangam[a]

[a] Department of Chemical and Petroleum Engineering, University of Calgary, Calgary, Canada, T2N 1N4

[b] Environmental & Property Solutions, Imperial Oil, Calgary, AB T2C 5N1, Canada.

Supplementary Information

Section S1. Electrostatic Repulsion Force Calculation

Electrostatic potential energy:

$$U = q * V_0 * e^{-r/\lambda d}$$

q = −e = -1.602×10^{-19}

V_0 = -20 mV (assuming)

r = 0.2 nm

λ_d = Debye length = 1/κ

$$\kappa = \sqrt{\frac{2e^2 I}{\varepsilon_0 \varepsilon_r K_B T}}$$

Assuming:

I = 0.01 M (Ionic strength),

ε_r = 78.5 (relative permittivity for water),

and T = 298 K, we have:

$$\lambda_d = \frac{1}{\kappa} = 3.04\ nm$$

$$U = 2.999 * 10^{-21} J = 1.81\ kJ/mol$$

Hydrogen bonding energies between $HCrO_4^-$ and nitrogen and oxygen functional groups are generally larger than 60 kJ/mol [1–3]. These values were obtained by theoretical approaches with Density Functional Theory (DFT) calculations that includes hydrogen bonding, Van der Waals interactions and electrostatic attraction/repulsions on molecular level.

Material	Specific Bonding	Adsorption Energy	Reference
Porous carbon modified with N and S through "Deep Eutectic Solvent Method"	- Hydrogen bond - Electrostatic attraction	Unmodified: ~ 16 kJ/mol S modified: ~ 26 kJ/mol N modified: ~ 60 kJ/mol N/S modified: ~ 75 kJ/mol	[1]
Mesoporous carbon sheet modified by N and/or S functional groups through hydrothermal process	- Hydrogen bond - Van der Waals interactions - Electrostatic attraction	S modified: 65 kJ/mol < E N modified: 80 kJ/mol < E N/S modified: 170 kJ/mol < E	[2]
Carbon nanotubes decorated with halloysite	- Hydrogen bond	N modified, O modified: ~ 80 kJ/mol	[3]

Section S2. Calculations regarding the role of pH and N functional groups in Cr(VI) reduction reactions as a removal mechanism

- pH = 5 → $[H^+] = 10^{-5}$ mol/L
  $N_{H+} = 10^{-5}$ mol/L × 0.1 L × 6.022×10^{23} ions/mol = 6.022×10^{17} (Number of H^+ ions in 0.1 L Sol)
- For N/S-GAC at pH_i = 5 and C_i = 50 ppm:
  q_e = 16.4 mg/g
  N_{Cr} = 16.4 mg/g × 1/1000 g/mg × 0.2 g × (1/52 mol/g) × 6.022×10^{23} ions/mol = 3.798×10^{19} (Number of Cr ions adsorbed on 0.2g adsorbent)
  Considering 50% reduction rate for the 1st adsorption cycle (based on UV-Vis, ICP and XPS analyses):
  $N_{Cr(III)} \approx 1.9 \times 10^{19}$
- For GAC at pH_i = 5 and C_i = 50 ppm:
  q_e = 10.4 mg/g
  N_{Cr} = 10.4 mg/g × 1/1000 g/mg × 0.2 g × (1/52 mol/g) × 6.022×10^{23} ions/mol = 2.409×10^{19} (Number of Cr ions adsorbed on 0.2g adsorbent)
  Considering 10% reduction rate for the 1st adsorption cycle (based on UV-Vis, ICP and XPS analyses):
  $N_{Cr(III)} \approx 2.4 \times 10^{18}$

Above calculations show that number of available H^+ from the solution is 30 times lower than the reduced Cr species for N/SGAC, and 4 times lower for GAC! Hence, H^+ should have been supplied from another source. We believe this source is protonated nitrogen species for N/S-GAC and possibly carboxylic groups in GAC.

CHNS analysis showed that N/S-GAC contains approximately 0.8 wt.% nitrogen after modification. Assuming that most of the nitrogen sites are protonated, a stoichiometric calculation for 0.2 g of N/S-GAC indicates that the available protons are sufficient to support the reduction of Cr(VI), corresponding to the consumption of approximately 3–4 H^+ per Cr(VI) reduced, consistent with the proposed amine-assisted reduction mechanism.

For 0.2 g N/S-GAC:

0.2 g × 0.8 % × (1/14 mol/g) × 6.022×10^{23} (atoms/mole) = 6.9×10^{19} atoms (Number of N atoms on GAC)

This is 3.6 times higher than $N_{Cr(III)}$.

A significant pH change occurs during adsorption, not only for N/S-GAC but also for unmodified GAC. Specifically, when the initial pH is 5.0 and the initial Cr(VI) concentration is 50 ppm, the final equilibrium pH values are ~7.2 for GAC and ~7.1 for N/S-GAC. This confirms that adsorption on both materials leads to a notable increase in solution pH.

This pH rise can be attributed to two main factors:

1. Proton consumption during the reduction of Cr(VI) to Cr(III), and
2. Accumulation of protons at the electrical double layer of the negatively charged surface under these conditions (Figure S3).

Similar calculations can be done at other pH values. Below, we have provided a table that includes final pH values from experiments regarding initial pH effect (Also included in section 2 in the supplementary information, page 3).

Table. Cr adsorption capacities and final pH of the solutions for GAC and N/S-GAC

Adsorbent	Initial pH	Adsorption Capacity (mg/g)	Final pH
GAC	3	20.5 ± 0.8	5.30 ± 0.21
	4	12.7 ± 0.4	6.83 ± 0.06
	5	10.6 ± 0.1	7.19 ± 0.10
	6	5.0 ± 1.5	7.16 ± 0.08
NSGAC	3	23.3 ± 0.4	5.41 ± 0.02
	4	16.7 ± 0.6	6.93 ± 0.02
	5	14.5 ± 0.6	7.13 ± 0.04
	6	11.8 ± 0.6	7.17 ± 0.03

Table S1. Mass balance analysis of Cr for the adsorption system and Cr speciation on adsorbents' surface by XPS

	Total Cr adsorbed (mg/g)	**Cr desorbed (mg/g)**					**Total Cr remained on adsorbent (mg/g)**
		KOH step		HCl step		**Total Cr desorbed (mg/g)**	Total Cr_{des} – Total Cr_{ads}
		Cr(VI)	Cr(III)	Cr(VI)	Cr(III)		
GAC	10.4 ± 0.2	9.3 ± 0.4	0.3 ± 0.4	0 ± 0.1	1.0 ± 0.1	10.6 ± 0.1	0 ± 0.2
N/S-GAC	16.4 ± 0.4	3.8 ± 0.4	5.2 ± 0.4	0 ± 0.1	2.4 ± 0.1	11.4 ± 0.2	5 ± 0.2

	Cr Species Composition on Adsorbent's Surface by XPS (%)			
	After Adsorption		**After KOH & HCl Desorption**	
	Cr(VI)	Cr(III)	Cr(VI)	Cr(III)
GAC	33	67	14	86
N/S-GAC	83	17	25	75

*Note: Formation of Cr(III) hydroxides on surface may lead to false results in XPS analysis and should be treated with caution. ICP-OES and UV-Vis analyses can give more reliable data, accounting for surface and bulk of the adsorbents.

Table S2. Adsorption isotherms: equations, parameters and description[4,5]

	Original Equation	Parameters	Description and Assumptions
Freundlich	$q_t = K_F C_e^{\frac{1}{n_f}}$	K_F: The Freundlich constant n_F: the dimensionless Freundlich intensity parameter, indicative of the surface heterogeneity	• Empirical model • Describes a mono- or multi-layer adsorption
Langmuir	$q_e = \frac{q_m K_L C_e}{1 + K_L C_e}$	K_L: the ratio of adsorption and desorption rate (L/mg) [5] q_m: Langmuir maximum adsorption capacity (mg/g)	• Theoretical model • Surface of adsorbent is homogeneous • All active sites are energetically the same and energy of adsorption is equal for all • Each site can hold only one molecule (monolayer coverage) • Interaction between adsorbate molecules on nearby sites is negligible • Describes adsorption on the surface with discrete adsorption sites • Describes monolayer homogeneous adsorption
Redlich-Peterson	$q_e = \frac{K_{RP} C_e}{1 + a_{RP} C_e^g}$	K_{RP}: a constant (L/g) A_{RP}: a constant g: an exponent between 0 and 1, if g=1 the model reduces to Langmuir, if g=0 or Ce approaches 0 the model reduces to linear, if Ce approaches to	• Hybrid model • An empirical hybrid of Langmuir and Freundlich models • Usually applied to homogenous or heterogenous adsorption systems

		infinity the model reduces to Freundlich	
Sips	$q_e = \frac{q_{ms} K_S C_e^{n_s}}{1 + K_S C_e^{n_s}}$	q_{ms}, is the maximum adsorption capacity (mg/g) K_s, is a constant ns, is a constant,	• Hybrid model • Adsorption is monolayer • An empirical hybrid of Langmuir and Freundlich models • Can describe monolayer, homogeneous or heterogeneous systems • If n_s=1 the model reduces to Langmuir • At low C_0 values the model reduces to Freundlich
Temkin	$q_e = \frac{RT}{b} ln(AC_e)$	R, is the ideal gas constant (J/mol*K) T, is the temperature (K) b, is a constant A, is a constant	• Empirical model • Adsorption is multilayer • The differential heat of adsorption was linearly decreased with surface coverage

Table S3. Isotherm parameters and fitting quality obtained from non-linear regression

Isotherm	**GAC**		**N/S-GAC**	
	Parameters ± Confidence Interval	**Fitting Quality**	**Parameters ± Confidence Interval**	**Fitting Quality**
Freundlich	K_F = 1.229 ± 0.882 n = 1.486 ± 0.341	R^2 = 0.966 SSE = 45.34	K_F = 3.914 ± 0.587 n = 2.092 ± 0.147	R^2 = 0.978 SSE = 29.997
Langmuir	K_L = 0.007 ± 0.001 q_m = 70.844 ± 2.364	R^2 = 0.992 SSE = 13.379	K_L = 0.018 ± 0.009 q_m = 56.821 ± 11.690	R^2 = 0.970 SSE = 52.904

Redlich-Peterson*	K_{RP} = 0.477 ± 0.285 a_{RP} = 0.007 ± 0.042 g = 1 ± 1.005	R^2 = 0.992 SSE = 13.379	K_{RP} = 5.308 ± 8.797 a_{RP} = 0.947 ± 2.088 g = 0.619 ± 0.284	R^2 = 0.979 SSE = 23.46
Sips*	q_{ms} = 46.946 ± 2.220 n_s = 1.449 ± 0.088 K_s = 0.002 ± 0.0002	R^2 = 0.999 SSE = 0.409	q_{ms} = 147.190 ± 182.144 n_s = 0.633 ± 0.344 K_s = 0.025 ± 0.026	R^2 = 0.980 SSE = 27.5
Temkin	a = 0.094 ± 0.022 b = 190.831 ± 24.65	R^2 = 0.979 SSE = 25.091	a = 0.35 ± 0.227 b = 250.07 ± 57.445	R^2 = 0.938 SSE = 84.679

*Note: The fitted parameters of the Redlich–Peterson for both adsorbents and Sips model for N/S-GAC exhibit large confidence intervals for N/S-GAC probably due to strong correlations among them.

Table S4. Adsorption kinetic models [4,6,7]

	Original Equation	Parameters	Descriptions and Assumptions
Pseudo-first Order	$q_t = q_e(1 - e^{-k_1 t})$	q_e: the equilibrium adsorption capacity K_1: is the PFO rate constant	• Reaction-Kinetic based model • Initial concentration of adsorbates is high and constant • Adsorption is in initial stage • A few active sites are on the adsorbent • Adsorption is considered irreversible and uses one active site per adsorbate
Pseudo-second Order	$q_t = \frac{q_e^2 k_2 t}{1 + q_e k_2 t}$	qe: the equilibrium adsorption capacity	• Reaction-Kinetic based model • Initial concentration of adsorbate is low and stays constant • Adsorption is in its final stage • Adsorbent is abundant with active sites

		k_2: the PSO rate constant (g/mg*h)	• Irreversible reaction, using two actives sites per adsorbate
Revised Pseudo-second Order	$q_n = q_{n-1} + ((t_n - t_{n-1}).\left(k'C_{t(n-1)}\left(1 - \frac{q_{n-1}}{q_e}\right)^2\right))$	q_e: the equilibrium adsorption capacity k': the r-PSO rate constant (L/g*min)	• Reaction-Kinetic based model • Adsorbate concentration does not stay constant
Elovich	$q_t = \frac{1}{b}\ln(1 + abt)$	a_e: the initial adsorption rate constant (mg/g*min) b_e: the rate of change of the activation every with surface coverage (g/mg)	• Reaction-Kinetic based model • Activation energy increased with time • Heterogeneous adsorbent surface • Originally developed for gas adsorption onto solid
Boyd-Reichberg	$\frac{q_t}{q_e} = \frac{6}{\pi^{3/2}}\sqrt{Bt} - \frac{3}{\pi^2}Bt$ $B = \frac{\pi^2 D_i}{r_p^2}$	q_t: the adsorption capacity (experimental data) q_e: the equilibrium adsorption capacity	• Mass transfer-Diffusion based model • Bulk Concentration does not change with time • No significant external resistance to mass transfer • Equilibrium follows a linear isotherm
Weber-Morris	$q_t = k_{wm}t^{0.5} + C$	K_{wm}: is the intraparticle diffusion rate constant C: a constant	• Mass transfer- diffusion based model • Follows all basic Boyd Model assumptions • Additionally, adsorbate concentrations inside adsorbent are low and at beginning of batch adsorption process (low values of time)

Table S5. Kinetics parameters and fitting quality obtained from non-linear regression*

Isotherm	GAC		N/S-GAC	
	Parameters ± Confidence Interval	**Fitting Quality**	**Parameters ± Confidence Interval**	**Fitting Quality**
Pseudo-first Order	K_1 = 0.019 ± 0.003 q_e = 10.586 ± 0.547	R^2 = 0.985 SSE = 3.534	K_1 = 0.015 ± 0.004 q_e = 12.048 ± 0.951	R^2 = 0.970 SSE = 8.228
Pseudo-second Order	K_2 = 0.002 ± 0.0003 q_e = 11.848 ± 0.406	R^2 = 0.995 SSE = 1.020	K_2 = 0.0014 ± 0.0003 q_e = 13.636 ± 0.577	R^2 = 0.995 SSE = 1.486
Revised Pseudo-second Order*	K’ = 0.0056 ± 0.0006 q_e = 11.94 ± 0.457	R^2 = 0.991 SSE = 1.534	K’ = 0.0055 ± 0.0004 q_e = 14.002 ± 0.412	R^2 = 0.997 SSE = 0.806
Elovich	a = 0.780 ± 0.475 b = 0.470 ± 0.092	R^2 = 0.960 SSE = 7.266	a = 0.683 ± 0.214 b = 0.395 ± 0.042	R^2 = 0.991 SSE = 2.083

*The revised PSO model has been chosen since it does not have the condition of constant concentration of adsorbate during the adsorption process.

Table S6. Kinetics parameters for > 200 min and fitting quality obtained from non-linear regression*

Isotherm	GAC		N/S-GAC	
	Parameters ± Confidence Interval	**Fitting Quality**	**Parameters ± Confidence Interval**	**Fitting Quality**
Pseudo-first Order	K_1 = 0.011 q_e = 11.108	R^2 = 0.835 SSE = 0.084	K_1 = 0.007 q_e = 13.281	R^2 = 0.835 SSE = 0.648
Pseudo-second Order	K_2 = 0.003 ± 2 x 10^{-5} q_e = 11.579 ± 0.005	R^2 = 0.999 SSE = 1.91 x 10^{-6}	K_2 = (8.86 ± 5.02)×10^{-4} q_e = 14.47 ± 1.139	R^2 = 0.981 SSE = 0.069
Revised Pseudo-second Order	K’ = 0.015 ± 0.007 q_e = 11.280 ± 0.162	R^2 = 0.994 SSE = 0.003	K’ = 0.006 ± 0.002 q_e = 13.999 ± 0.298	R^2 = 0.999 SSE = 0.025
Elovich	a = 137095.05 ± 1637700 b = 1.713 ± 1.169	R^2 = 0.952 SSE = 0.024	a = 6.33 ± 9.47 b = 0.615 ± 0.014	R^2 = 0.994 SSE = 0.021

* These data seem unreliable due to low number of data points after 200 minutes (only 4 points).

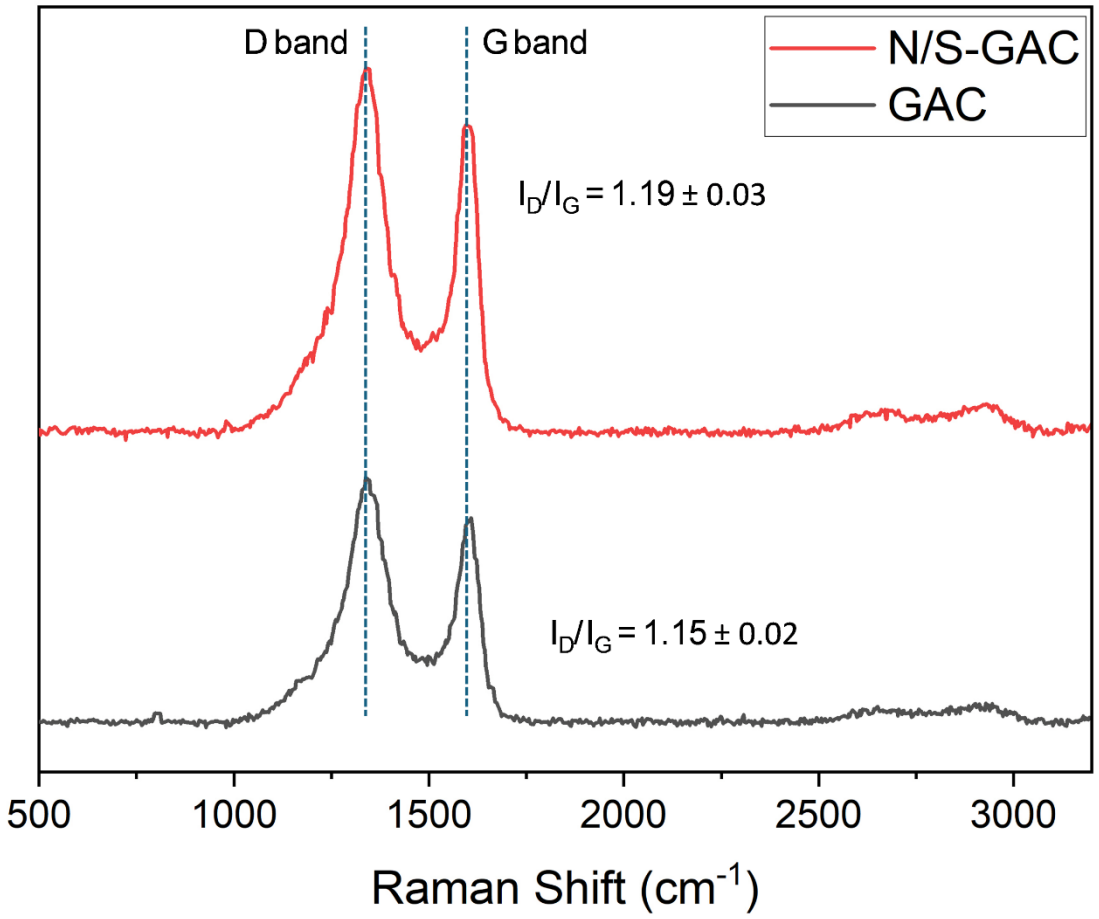

Figure S1. Raman spectra of GAC and N/S-GAC.

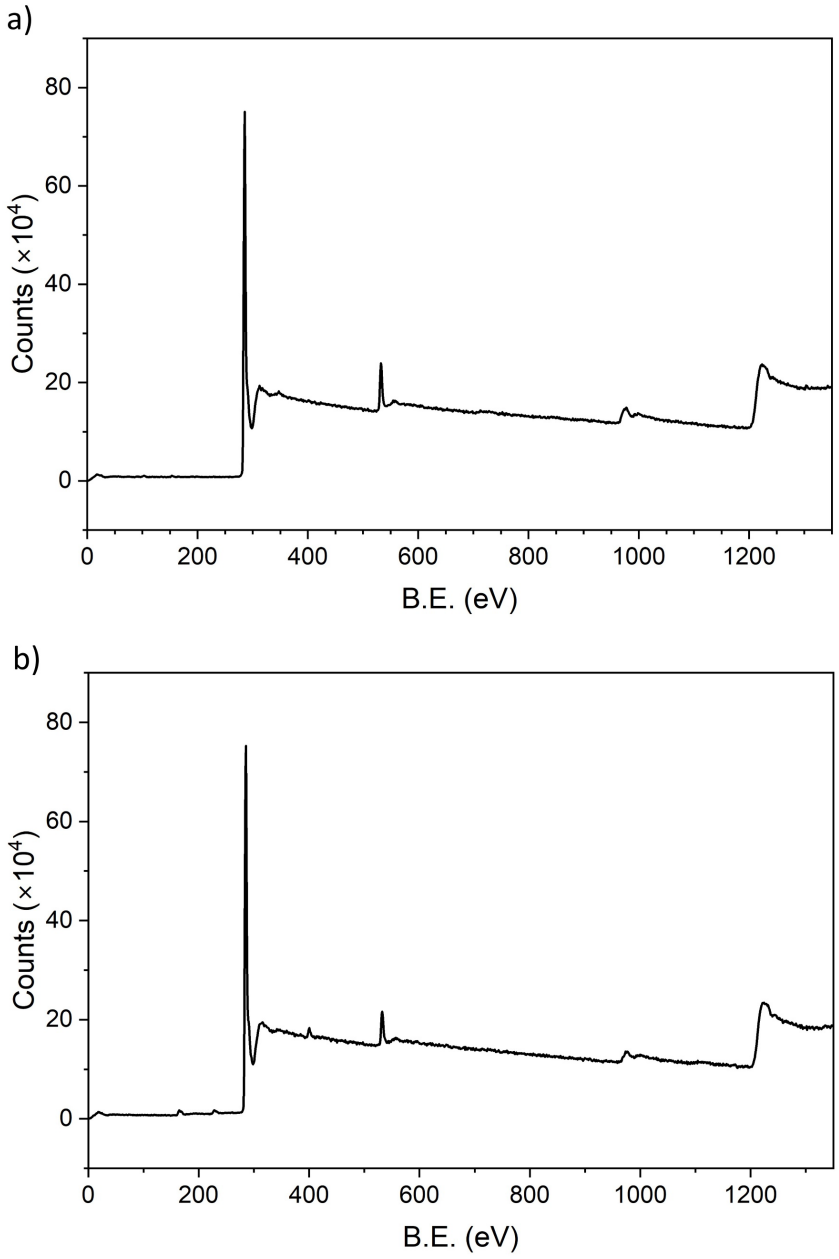

Figure S2. XPS survey spectra of a) GAC and b) N/S-GAC.

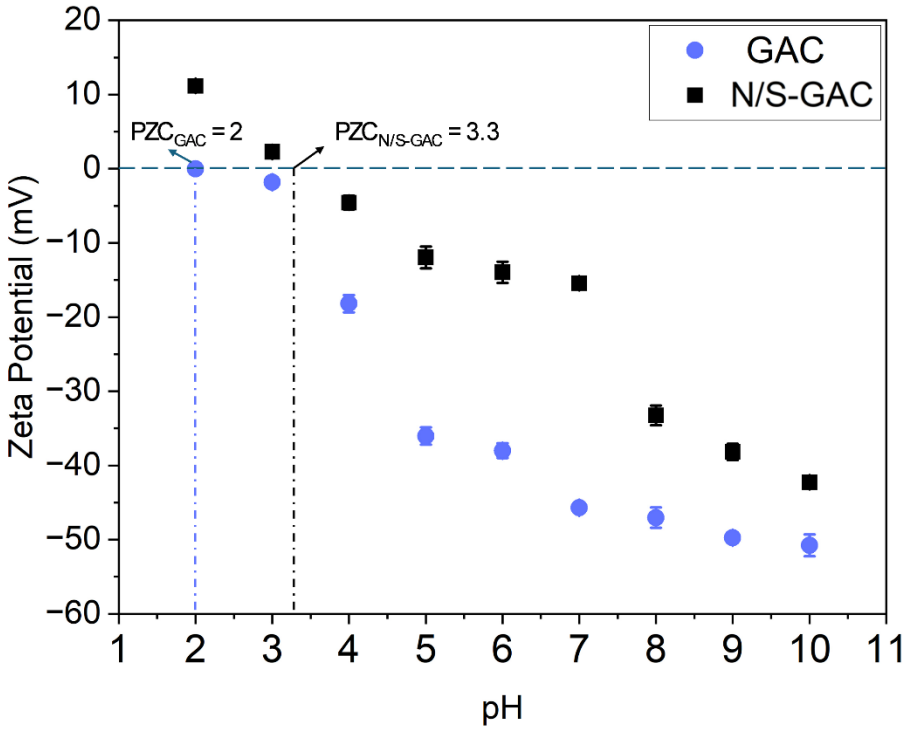

Figure S3. Zeta potential vs. pH plots for GAC and N/S-GAC.

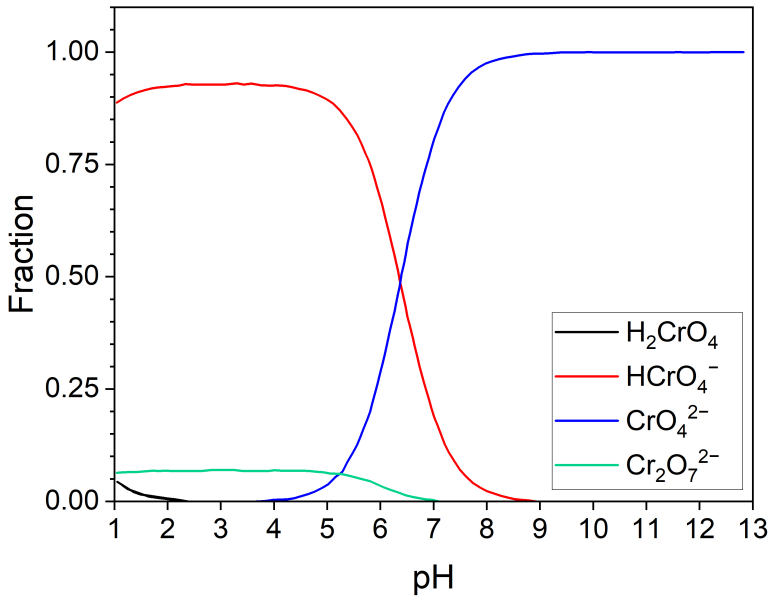

Figure S4. Speciation diagrams of a) Cr(VI) and b) Cr(III), obtained from Hydra-Medusa software (Conditions: C_{Cr} = 0.001 M, can_{+} = 0.01 M, C_{Cl^-}= 0.01 M, pH = 1-13, log(pCO_2) = -3.5, Ioni Strength = 0.01 M.

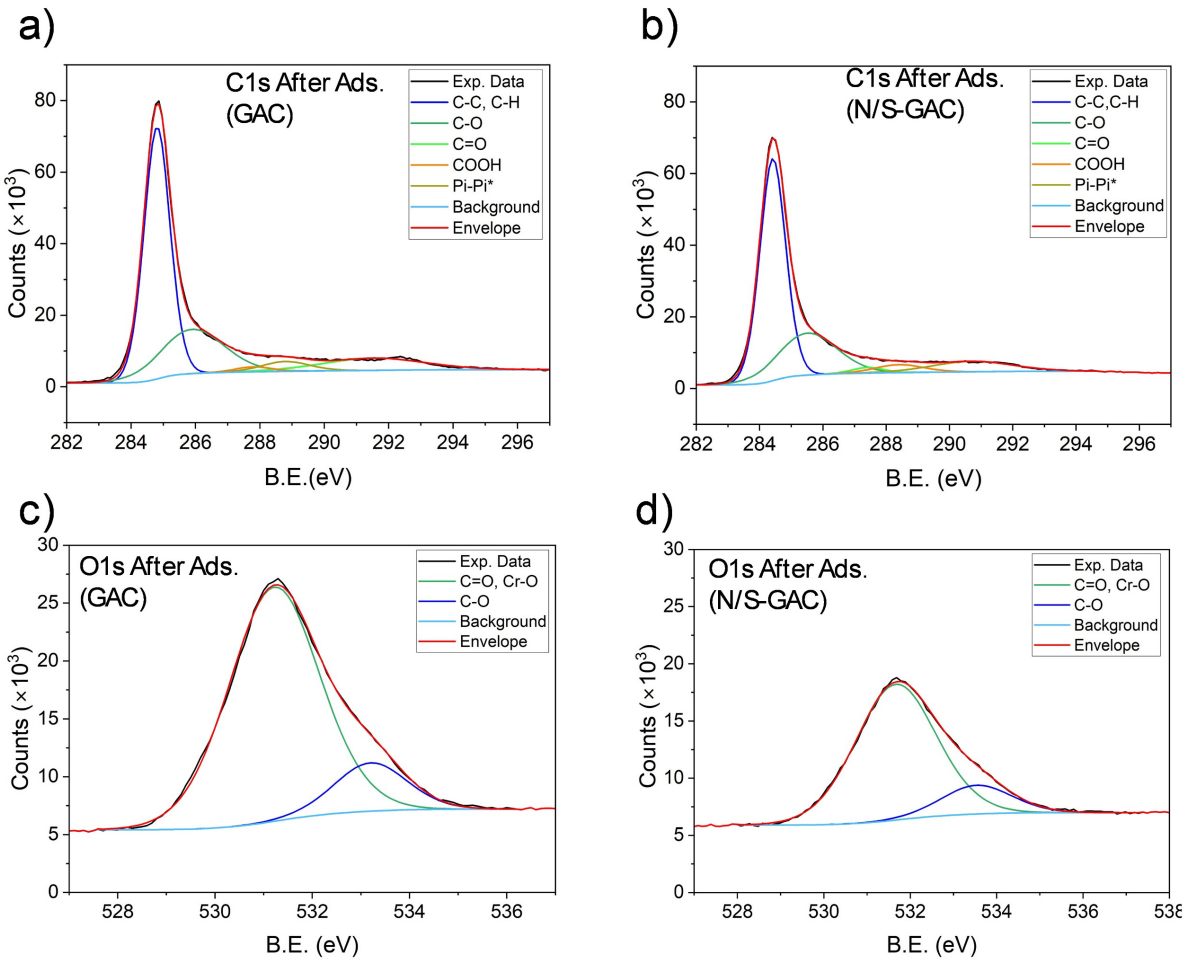

Figure S5. XPS spectra of GAC and N/S-GAC after adsorption: a) C1s GAC, b) C1s N/S-GAC, c) O1s and d) O1s N/S-GAC (pH_i = 5, C_i = 50 ppm, t = 20 h, adsorbent dosage = 2 g/L).

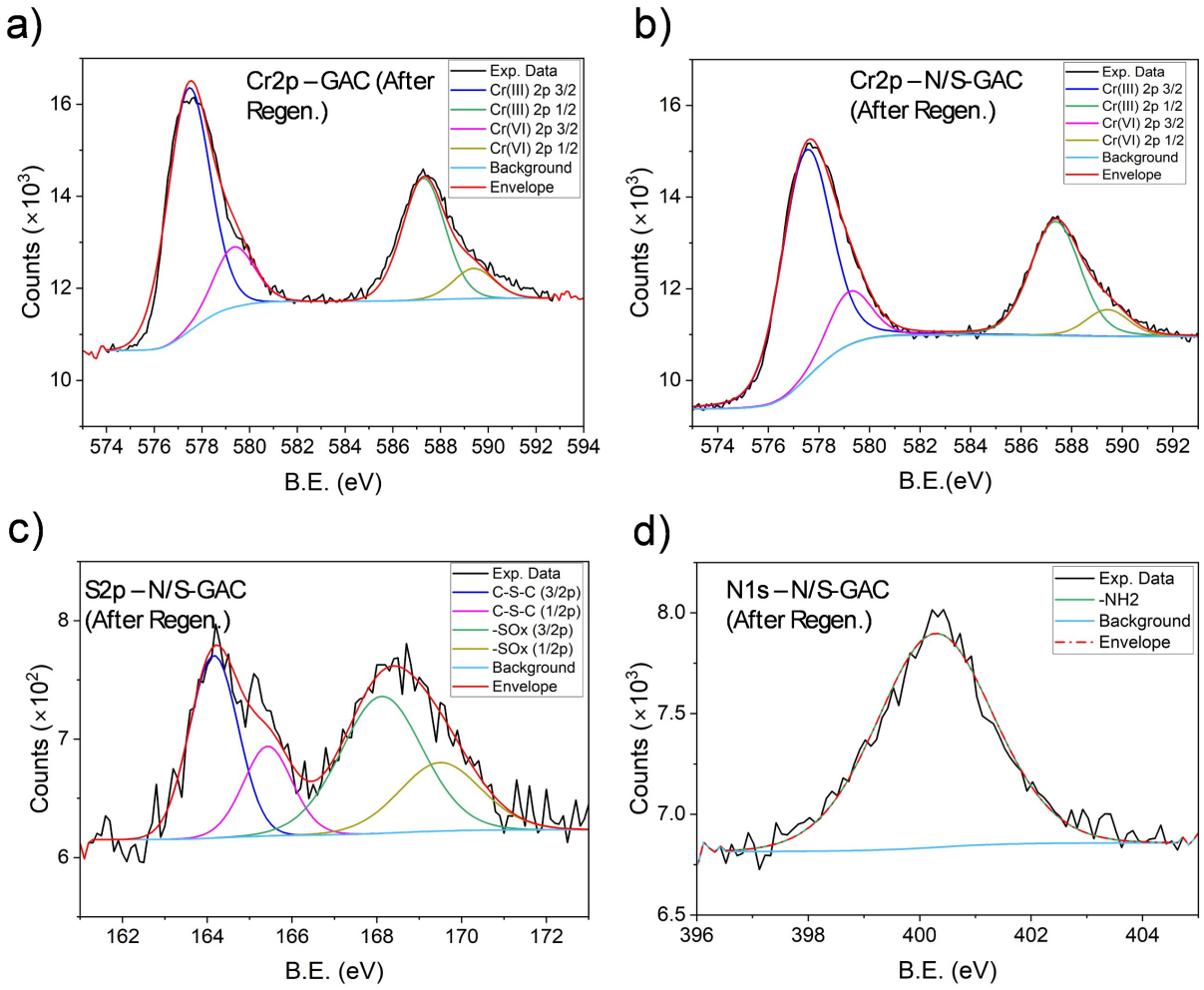

Figure S6. XPS data for regenerated GAC and N/S-GAC: a) Cr2p GAC, b) Cr2p NSGAC, c) S2p N/S-GAC, d) N1s N/S-GAC (Regeneration Condition: two steps of alkaline regeneration, each with 50 ml of 0.1 M KOH solution, t = 8h, T = room temperature).

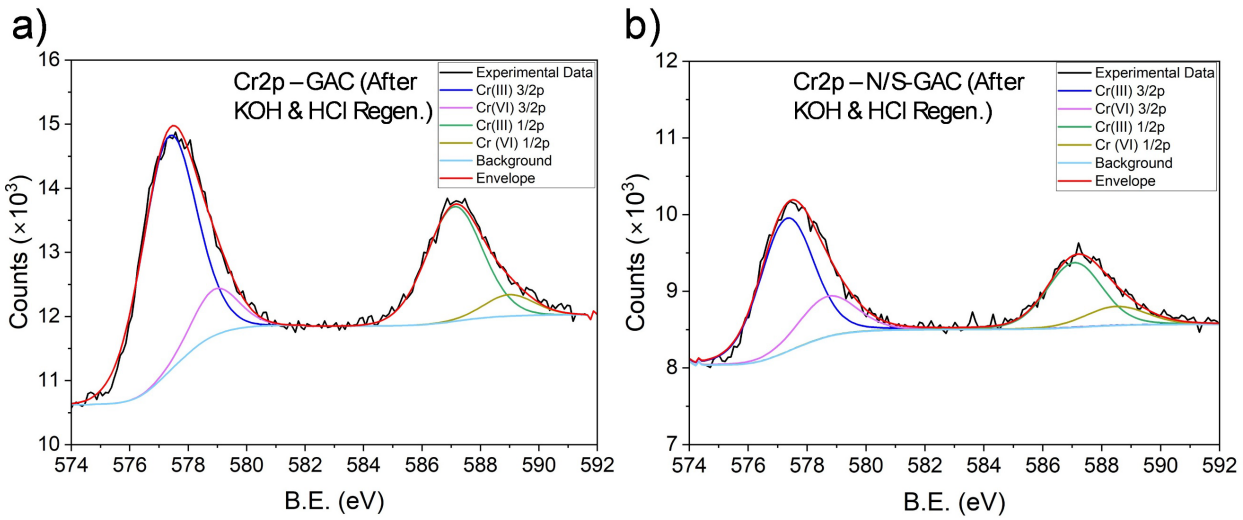

Figure S7. XPS data for regenerated GAC and N/S-GAC after both KOH and HCl regeneration: a) Cr2p GAC, b) Cr2p NSGAC (Regeneration Condition: two steps of alkaline regeneration, each with 50 ml of 0.1 M KOH solution, t = 8h, T = room temperature, followed by one step of acidic regeneration, with 50 ml of 1 M HCl, t = 8h, T = room temperature).

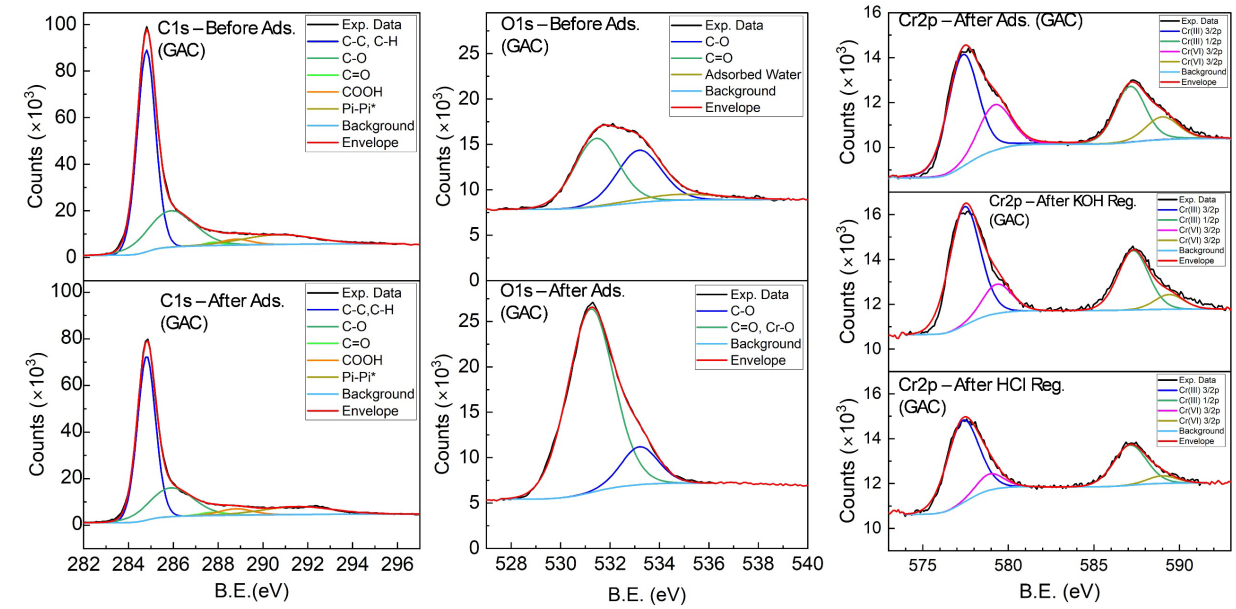

Figure S8. XPS spectra of GAC including the count numbers as a reference for C1s, O1s and Cr2p.

Note: The adsorbent granules used in this study (GAC and N/S-GAC) differ in surface roughness, packing density, and pore orientation, all of which can influence the local surface chemistry and the number of photoelectrons escaping toward the detector. Such geometric and topographical variations alter the effective sampling depth and signal intensity, making the absolute count values dependent on the sample morphology rather than being intrinsic material properties. Therefore, cross-sample comparisons based on absolute count numbers should be approached with caution.

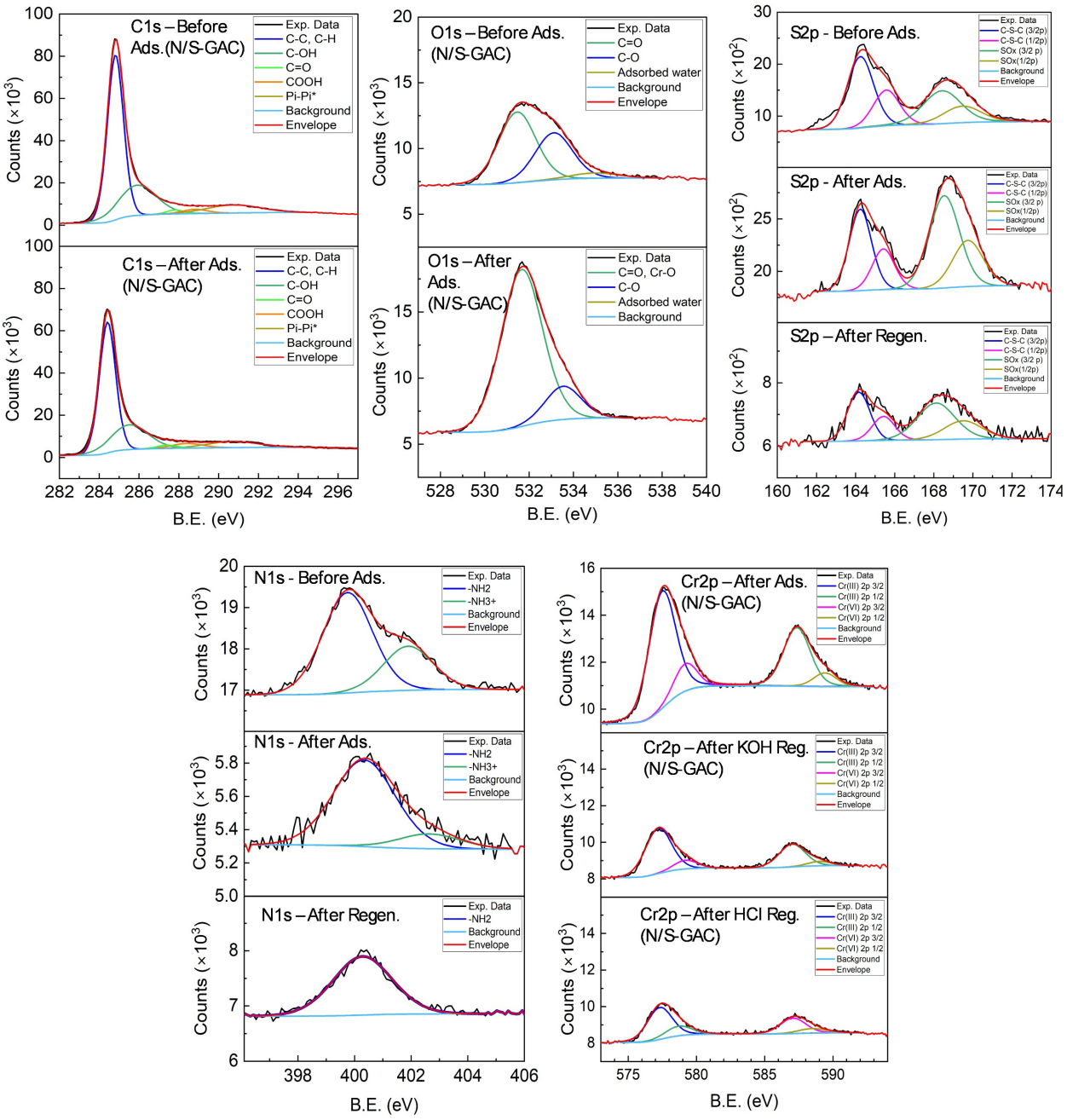

Figure S9. XPS spectra of N/S-GAC including the count numbers as a reference for C1s, O1s and Cr2p.

Note: The adsorbent granules used in this study (GAC and N/S-GAC) differ in surface roughness, packing density, and pore orientation, all of which can influence the local surface chemistry and the number of photoelectrons escaping toward the detector. Such geometric and topographical variations alter the effective sampling depth and signal intensity, making the absolute count values dependent on the sample morphology rather than being intrinsic material properties.

Therefore, cross-sample comparisons based on absolute count numbers should be approached with caution.

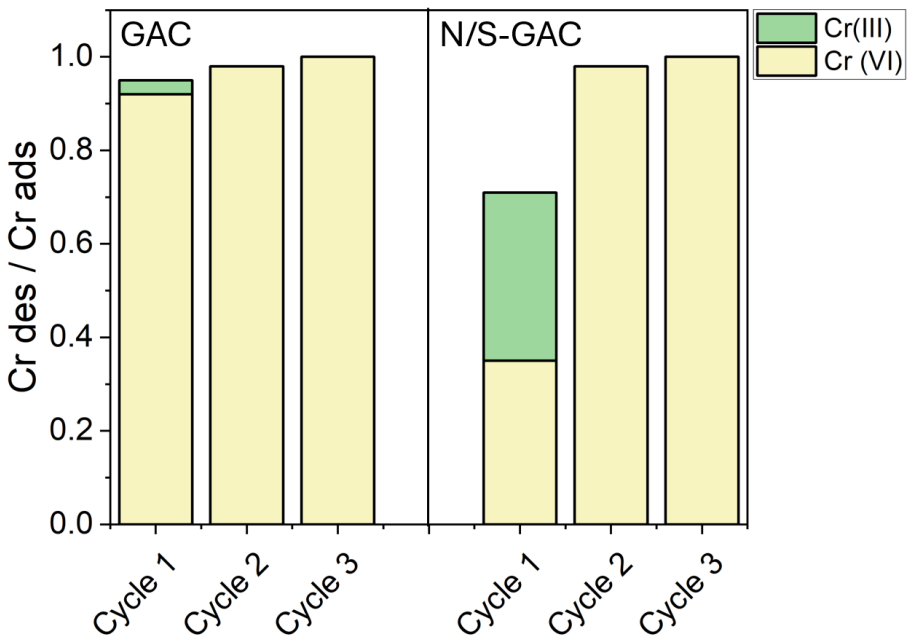

Figure S10. Amount of Cr(VI) and Cr(III) desorbed in each cycle with respect to the total Cr adsorbed in each cycle.

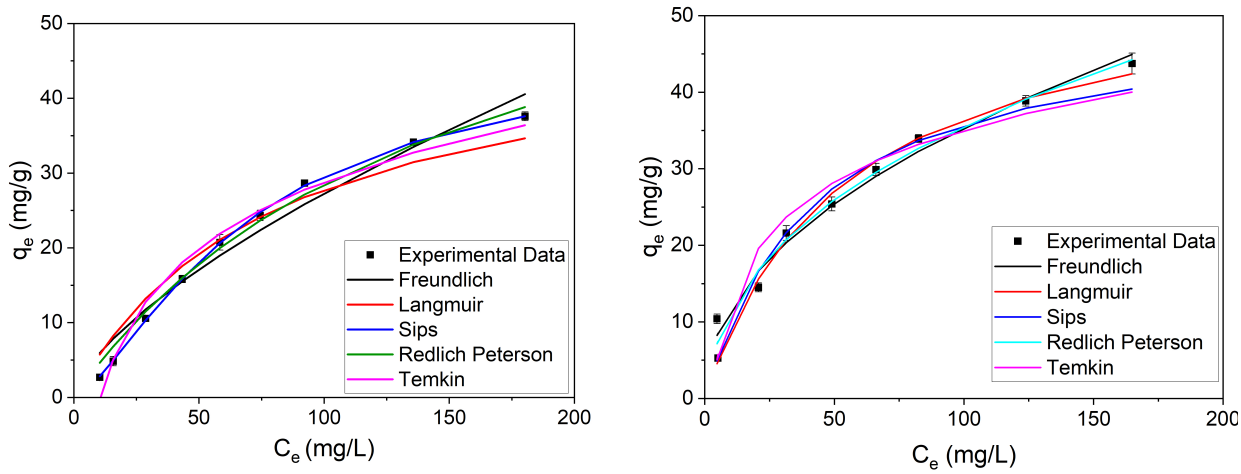

Figure S11. Experimental data and the fitted isotherms: a) GAC, b) N/S-GAC.

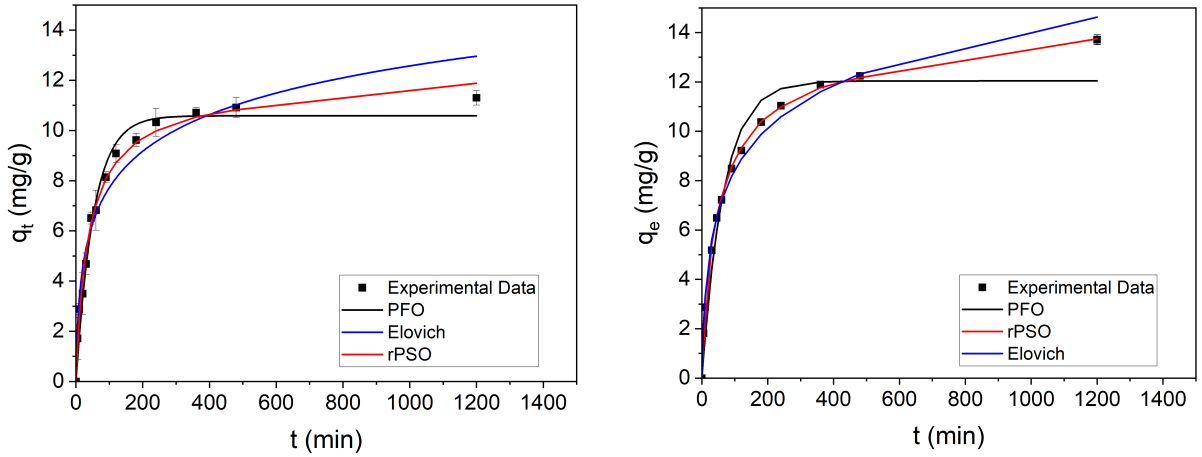

Figure S12. Experimental data and the fitted kinetic models: a) GAC and b) N/S-GAC.

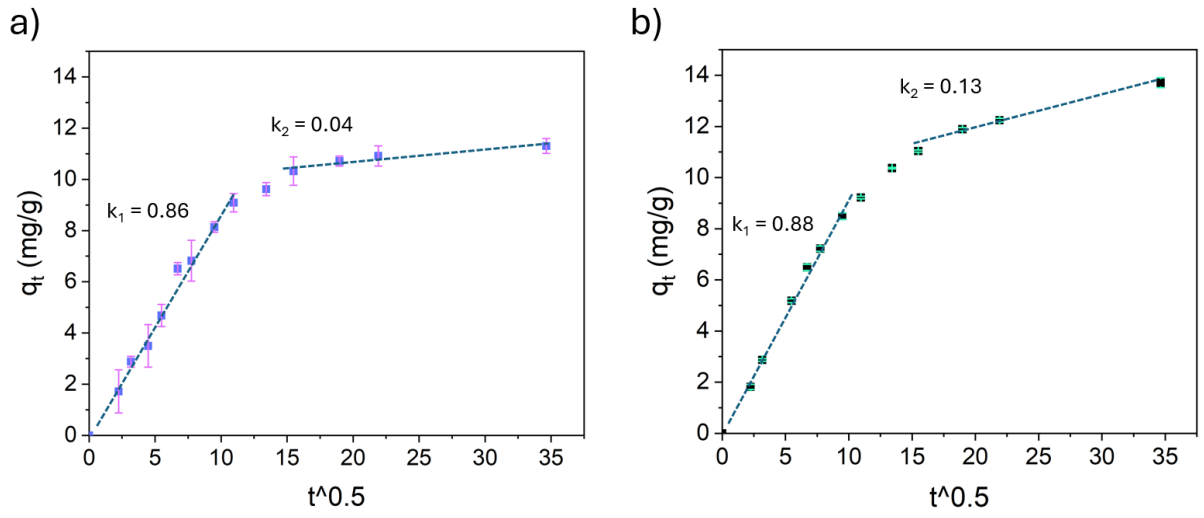

Figure S13. Weber-Morris model for: a) GAC and b) N/S-GAC.

References

1 J. Chen, M. Yuan, W. Cai, J. Wei, J. Zhou, P. Liu, Z. Yang, J. Luo, Q. Xia and Z. Cai, *Chemical Engineering Journal*, 2021, **422**, 130153.

2 F. Chen, M. Zhang, L. Ma, J. Ren, P. Ma, B. Li, N. Wu, Z. Song and L. Huang, *Science of The Total Environment*, 2020, **730**, 138930.

3 S. N. Ahmad Shah, S. Zulfiqar, F. Ruipérez, M. Rafique, M. Iqbal, M. J. Forrester, M. I. Sarwar (Late) and E. W. Cochran, *RSC Adv.*, 2024, **14**, 2947–2960.

4 Y. Wang, C. Wang, X. Huang, Q. Zhang, T. Wang and X. Guo, *Chemosphere*, 2024, **349**, 140736.

5 K. H. Chu, M. A. Hashim, Y. T. D. C. Santos, J. Debord, M. Harel and J.-C. Bollinger, *Chemical Engineering Science*, 2024, **285**, 119573.

6 J. C. Bullen, S. Saleesongsom, K. Gallagher and D. J. Weiss, *Langmuir*, 2021, **37**, 3189–3201.

7 Q. Hu, S. Ma, Z. He, H. Liu and X. Pei, *Journal of Water Process Engineering*, 2024, **60**, 105241.